Optical Action Potential Upstroke Morphology Reveals Near-Surface Transmural Propagation Direction

Christopher J. Hyatt, Sergey F. Mironov, Frederick J. Vetter, Christian W. Zemlin, Arkady M. Pertsov

***Abstract*—**The analysis of surface-activation patterns and measurements of conduction velocity in ventricular myocardium is complicated by the fact that the electrical wavefront has a complex 3D shape and can approach the heart surface at various angles. Recent theoretical studies suggest that the optical upstroke is sensitive to the subsurface orientation of the wavefront. Our goal here was to (1) establish the quantitative relationship between optical upstroke morphology and subsurface wavefront orientation using computer modeling and (2) test theoretical predictions experimentally in isolated coronary-perfused swine right ventricular preparations. We show in numerical simulations that by suitable placement of linear epicardial stimulating electrodes, the angle ϕ of wavefronts with respect to the heart surface can be controlled. Using this method, we developed theoretical predictions of the optical upstroke shape dependence on ϕ. We determined that the level V_F* at which the rate of rise of the optical upstroke reaches the maximum linearly depends on ϕ. A similar relationship was found in simulations with epicardial point stimulation. The optical mapping data were in good agreement with theory. Plane waves propagating parallel to myocardial fibers produced upstrokes with V_F*<0.5, consistent with theoretical predictions for $\phi>0$. Similarly, we obtained good agreement with theory for plane waves propagating in a direction perpendicular to fibers (V_F*>0.5 when $\phi<0$). Finally, during epicardial point stimulation, we discovered characteristic saddle-shaped V_F* maps that were in excellent agreement with theoretically predicted changes in ϕ during wavefront expansion. Our findings should allow for improved interpretation of the results of optical mapping of intact heart preparations. **(*Circ Res*. 2005;97:277-284.)**

Key Words: optical action potential ■ conduction velocity ■ optical mapping ■ voltage-sensitive dye

Patterns of electrical activation within the ventricular wall are determined in large part by the specific 3D organization of myocardial fibers. Histological studies of intact hearts from many species have shown conclusively that myocardial fiber orientation rotates significantly across the heart wall.[1] The total angle of rotation across the myocardial wall can reach 180°.[2] Because of the complex transmural organization of myocardial fibers, an excitation wavefront typically assumes a complex 3D profile that, depending on the mode of stimulation, can approach the myocardial surface at a variety of different angles.[3–6] For this reason, obtaining accurate quantitative information about the wavefront orientation with respect to the surface is quite important for the interpretation of surface recordings, particularly with regard to measurements of conduction velocity.

In a recent modeling study,[7] we discovered that the upstroke morphology of optical action potentials (OAPs) was sensitive to the local subsurface orientation of the excitation wavefront. This suggests that analysis of OAP upstroke morphology may prove useful in determining subsurface wavefront orientation. The goals of this study were (1) to establish the quantitative relationship between OAP upstroke morphology and subsurface wavefront orientation and (2) to test the predictions of the model experimentally.

Our first objective was to develop an experimentally feasible procedure for producing excitation fronts with various orientations with respect to the surface. In the computer-modeling section of this study, we predicted that this objective could be achieved by appropriate positioning of a linear stimulation electrode in the epicardial plane. In particular, our simulations predicted that by initiating a stationary plane wave either parallel or perpendicular to myocardial fibers, one can produce, respectively, an excitation wavefront with either a positive (+20.7°) or negative (−58.9°) orientation with respect to the heart surface. Intermediate wavefront orientations can then be obtained by selecting intermediate positions for the linear stimulation electrode with respect to the surface fiber direction. Using this approach, we established a theoretical, quantitative relationship between the OAP upstroke morphology and the angle, ϕ, between the normal to the excitation front and the myocardial surface. Specifically, our simulations predicted that the level (V_F*) at

Original received April 1, 2003; first resubmission received November 11, 2004; second resubmission received February 24, 2005; revised second resubmission received June 8, 2005; accepted June 21, 2005.

From the Department of Pharmacology (C.J.H., S.F.M., C.W.Z., A.M.P.), State University of New York, Upstate Medical University, Syracuse; and the Biomedical Engineering Program (F.J.V.), Department of Electrical and Computer Engineering, University of Rhode Island, Kingston.

Correspondence to Arkady M. Pertsov, PhD, SUNY Upstate Medical University, Dept of Pharmacology, 750 E Adams St, Syracuse, NY 13210. E-mail perzova@upstate.edu

Circulation Research **is available at http://circres.ahajournals.org** **DOI: 10.1161/01.RES.0000176022.74579.47**

which the rate of rise of the OAP reaches the maximum is linearly related to the optically weighted mean angle of the excitation wavefront with respect to the heart surface ($\bar{\phi}$). A similar relationship was found in simulations of epicardial point stimulation, in which the resulting excitation wavefront has a subsurface orientation that changes continuously during propagation.

The goal of second part of this study was to verify these theoretical predictions through analysis of optical mapping experiments in isolated swine right ventricle preparations. In these experiments, we examined OAP upstroke morphologies for wavefronts produced by both line stimulation (parallel and perpendicular to epicardial fibers) and point stimulation (epicardial and endocardial). We discovered that plane waves propagating along myocardial fibers produced upstrokes such that $V_F^*<0.5$, which was consistent with the theoretical prediction for negative subsurface angles. Similarly, good agreement with the theory (ie, $V_F^*>0.5$) was obtained for plane waves propagating in perpendicular direction with positive subsurface angles. Finally, during epicardial point stimulation, we discovered characteristic saddle-shaped V_F^* maps that were in excellent agreement with theoretically predicted changes in the subsurface wavefront angle during its expansion. Our experimental findings support the hypothesis that OAP upstroke morphology indicates subsurface wavefront orientation.

Materials and Methods

Isolated Coronary-Perfused Pig Right Ventricular Preparation

All experimental protocols conformed to the *Guide for the Care and Use of Laboratory Animals* (NIH publication No. 85-23, revised 1996). Young pigs (n=8; Keystone Mills, Romulus, NY) were heparinized (500 IU, IV) and anesthetized with sodium pentobarbital (35 mg/kg IV). The heart was rapidly removed and Langendorff-perfused with cold (4°C) cardioplegic solution (in mmol/L: 280 glucose, 13.44 KCl, 12.6 $NaHCO_3$, 34 mannitol). The right free ventricular wall was quickly excised, and the right coronary artery was cannulated. Nonperfused tissue was removed, and the preparation was stretched on a plastic frame. Preparations were perfused via the right coronary artery with a standard oxygenated (95% O_2/5% CO_2) Tyrode's solution (pH 7.4, 37°C) at a pressure of 80 mm Hg and superfused with the same solution at a rate of 40 mL/min. Diacetyl-monoxime was added to the Tyrode's solution (15 mmol/L) to stop contractions. The tissue was stained with the potentiometric dye di-4-ANEPPS (15 μg/mL) via the perfusate at the beginning of the experiment. The preparation was paced with unipolar electrodes, using either the tip of an insulated silver wire (point stimulation) or a length of bare silver wire sutured to the epicardium (line stimulation) using 5-ms duration pulses at a basic cycle length of 500 ms at 2× diastolic threshold.

Optical Setup

The optical setup consisted of a high-frame-rate charge-coupled device video camera (12-bit digital; Dalsa) with a Computar H1212FI lens (focal length 12 mm, 1:1.2 aperture ratio; CBC Corp, Commack, NY). A collimated beam provided by a 250 W tungsten halogen lamp uniformly illuminated the epicardial surface of the preparation. The light was heat filtered and then passed through bandpass 520±40 nm excitation filters. Fluorescence was recorded at 640±50 nm. The video images (64×64 pixels) were acquired from an ≈22×22 mm area of the preparation at either 608 or 913 frames per second. The background fluorescence was subtracted from each frame to obtain the voltage-dependent optical signal.

Processing of Optical Recordings

In all experiments, from 50 to 100 OAPs from each recording were ensemble averaged to reduce noise, thereby avoiding the use spatial or temporal filters that might affect OAP upstroke morphology. To allow temporal alignment and subsequent averaging of successive paced action potentials, the trigger for the pacing stimulus was recorded as a single pixel in the movie frames. The alignment error was no more than one-half frame (<0.8 ms).

To characterize the OAP upstroke morphology, we used the relative fractional level V_F^* at which the maximum time derivative of the voltage-sensitive fluorescence, $(\dot{V}_F)_{max}$, occurred. To obtain accurate estimates of V_F^*, we used cubic spline interpolation (5 additional points per interval) between actual data points in our time-series fluorescence data $V_F(t)$. Spatial variations in OAP upstroke morphology were presented as V_F^* maps.

Computer Simulations

To simulate electrical activity in the heart, we used the Fenton–Karma ionic model with Luo–Rudy phase-1 type restitution properties.[8] The geometry of our model was 32 mm×32 mm×8 mm, the approximate size of our isolated swine right ventricle preparations. The equation used to describe electrical activity in the slab is

$$\partial_t V_m = -I_{ion}/C_m + \nabla\cdot\tilde{D}\nabla V_m \quad (1)$$

where V_m is the transmembrane potential, C_m is the membrane capacitance, I_{ion} is the total ionic current density of the membrane, and $\tilde{D}$ is the diffusivity tensor. (For more details, see the online data supplement, available at http://circres.ahajournals.org.) Neumann no-flux boundary conditions were imposed at all tissue boundaries, that is, $\hat{n}\cdot(\tilde{D}\nabla V) = 0$, where $\hat{n}$ is the unit vector normal to the boundary.[8,9] The fibers were assumed to rotate at a linear rate with depth.[1] The total transmural rotation was set at 180°.[2,10] The diffusivity tensor $\tilde{D}$, was scaled to produce steady-state plane wave conduction velocities of 56.1 cm/s and 16.7 cm/s in the longitudinal and transverse directions, respectively, which was consistent with the values reported in swine epicardium.[11]

To calculate the voltage-dependent fluorescence signal, V_F, at the heart surface, we used a recently developed 2-stage model[7] that combines a 3D distribution of transmembrane voltage $V_m(\vec{r}, t)$ with a photon transport model. At a given point on the heart surface, V_F is determined by convolution of the transmembrane potential at each point within the heart tissue with an optical weighting function. The optical weighting function describes both the excitation and emission of voltage-sensitive fluorescence within heart tissue, including photon scattering and absorption. (See Hyatt et al[7] and the online data supplement for more detail.) Optical action potentials were computed over a 22×22 mm region on the epicardium, which represents the typical field of view of the video camera in our optical mapping experiments.

Results

OAP Upstroke Dependence on Subsurface Wavefront Orientation: Model Studies

Plane Stimulation

To test the hypothesis that OAP recordings can be used to determine the local subsurface wavefront orientation, we developed a method for reproducibly initiating excitation waves with various orientations with respect to the epicardium. As described below, this was achieved in both model and experiment using linear epicardial electrodes. We produced propagating "plane" wavefronts with specific steady-state subsurface orientations simply by changing the alignment of these linear electrodes on the epicardium.

Figure 1 (left) depicts the 3D organization of 2 steady-state "plane" wavefronts, initiated by linear epicardial stimulation in a direction longitudinal and transverse to surface fibers,

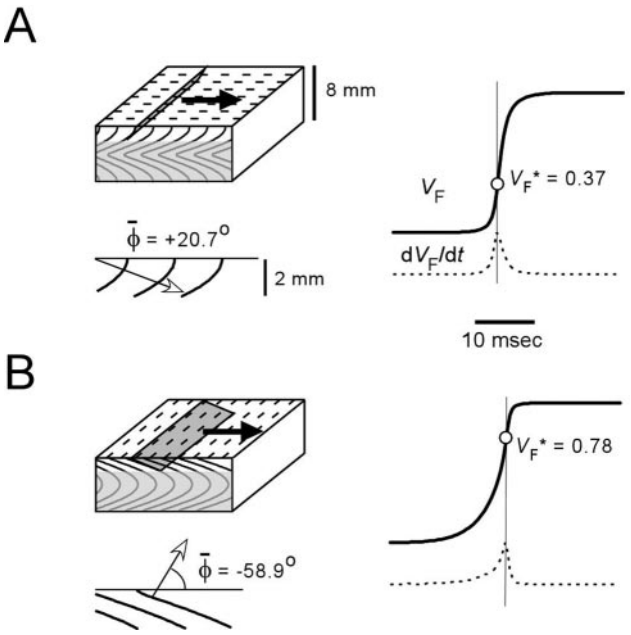

Figure 1. Controlling subsurface wavefront orientation. Computer simulations in a 3D slab of myocardial tissue with transmural fiber rotation. A (left), Wavefront propagates in the direction of epicardial fibers (indicated by dashed lines). Transmural isochrones are depicted on the side of the slab. Enlarged subsurface isochrone map is shown below. Arrow indicates the direction of the mean voltage gradient vector in subsurface layer (optically weighted mean angle, $\bar{\phi}$=20.7°). B (left), Excitation front propagates perpendicular to epicardial fibers. The angle, $\bar{\phi}$, for this case is −58.9°. The notations are the same as in A. A and B (right), OAP upstroke morphology and location of V_F* for the simulations in A (V_F*=0.37) and B (V_F*=0.78), respectively.

respectively. Note the significant difference in subsurface wavefront orientation produced by the 2 modes of stimulation. When observed in any given 2D plane parallel to the heart surface, the propagating fronts appear as true plane waves. Because of transmural fiber rotation, however, the intramural profiles of such propagating "plane" waves are quite complex and are sensitive to the direction of propagation. In the first example (Figure 1A), the wavefront has a positive angle ($\bar{\phi}$=20.7°) with respect to the surface. The magnitude of $\bar{\phi}$ represents the optically weighted mean. (For a precise definition of $\bar{\phi}$, see the online data supplement.) For the case of transverse propagation (Figure 1B), $\bar{\phi}$=−58.9° is negative, indicating a wavefront oriented toward the surface. By placing the electrode at transitional angles between those depicted in Figure 1, we obtained intermediate values of $\bar{\phi}$ (see online Table I). To produce wavefronts where $\bar{\phi}$=−90.0° and 0.0°, we performed 2 simulations in which we stimulated the whole endocardial ($\bar{\phi}$=−90.0°) and epicardial ($\bar{\phi}$=0.0°) surfaces.

By producing excitation waves with various orientations with respect to the epicardium, we established the quantitative relationship between OAP upstroke morphology and $\bar{\phi}$. To characterize the optical upstroke morphology we used a parameter V_F*, which represents the fractional level OAP at which the maximum time derivative of the voltage-sensitive fluorescence, $(\dot{V}_F)_{max}$, occurred (Figure 1, right panel). Larger V_F* values correspond to slower foot of the OAP.

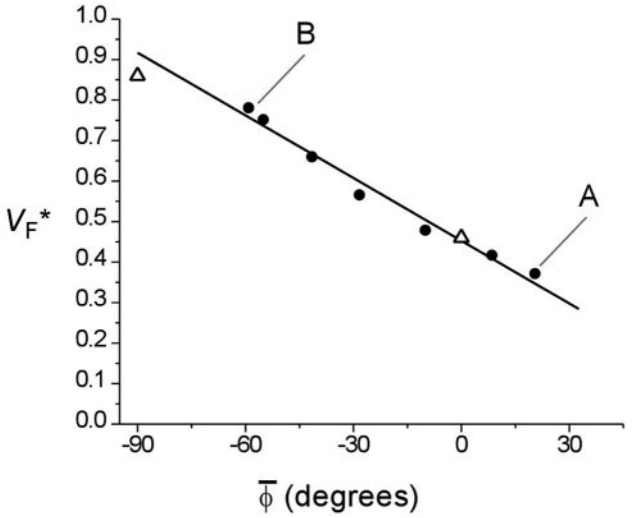

Figure 2. Relationship between V_F* and the optically weighted mean angle, $\bar{\phi}$, for steady-state subsurface wavefronts. The 2 open triangles represent simulations in which the excitation fronts propagated in the lateral ($\bar{\phi}$=0°) and transmural (endo- to epicardial) ($\bar{\phi}$=−90°) directions. The closed circles represent data for steady-state lateral plane wavefronts. The solid line represents the best linear regression fit to the data for steady-state lateral plane wavefronts. The data where the lateral plane wavefront propagated in the longitudinal and transverse surface fiber directions are denoted by A and B, respectively.

Figure 2 is a plot of V_F* versus $\bar{\phi}$ for angles ranging from −90° to 20.7°. The plot shows a linear correlation between the orientation of the excitation wavefront and the optical upstroke morphology over the entire range of $\bar{\phi}$. The equation of the best linear fit to the data yields V_F*=(0.47/90°)$\bar{\phi}$+0.45 with a correlation coefficient R=−0.99. The case where V_F*≈0.5 roughly defines the division point between conditions in which the wavefront propagates either toward (V_F*>0.5) or away from (V_F*<0.5) the heart surface. The strong correlation between V_F* and $\bar{\phi}$ indicates that OAP upstroke morphology is an excellent predictor of the subsurface orientation of excitation wavefronts with respect to heart surface.

Point Stimulation

In the previous section, we established the quantitative relationship between OAP upstroke morphology and $\bar{\phi}$ for steady-state propagating plane waves. To examine the correlation of V_F* and $\bar{\phi}$ during non–steady-state wave propagation, we chose the case of point stimulation. The diagram in Figure 3A depicts the evolution of the propagating wavefront after epicardial point stimulation in a slab of heart tissue with clockwise transmural fiber rotation. The wavefronts as they appear on the epicardium are roughly elliptical, with clockwise rotation of the expanding quasi-ellipses in the direction of the transmural fiber rotation. The transmural profiles in the diagram (see cutaway in Figure 3A) show a gradual change in the orientation of the excitation front with respect to the surface as it propagates away from the stimulation site. As the wave moves away from stimulation site in the epicardial transverse fiber direction, the sign of $\bar{\phi}$ changes from positive to negative.

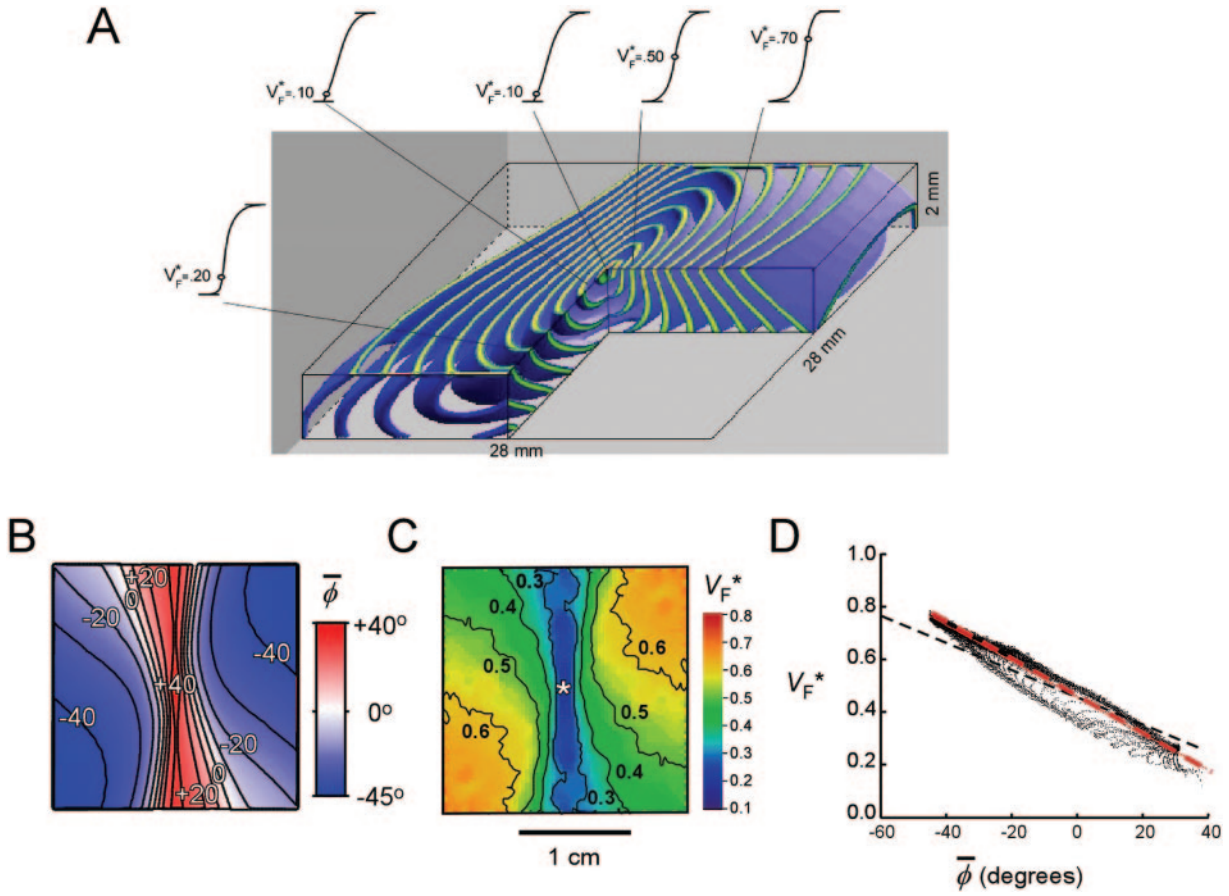

Figure 3. Subsurface wavefront orientation and spatial variation in OAP upstroke morphology after epicardial point stimulation. A, Simulated epicardial and transmural (cutaway) isochrone maps (interval, 5 ms). The corresponding OAP upstrokes at 5 different sites are shown (left and top). Open circles on the OAP upstrokes indicate the location of V_F*. B, Map of the optically weighted mean angle, $\bar{\phi}$, for this simulation (isolines of $\bar{\phi}$ are indicated). C, Corresponding V_F* map, with isolines of V_F* indicated. D, Plots showing the relationship between V_F* vs $\bar{\phi}$ at all corresponding pixels in the $\bar{\phi}$ and V_F* maps in B and C, respectively. The thick dashed red line is the linear regression of V_F* vs $\bar{\phi}$. For comparison, the thin black dashed line shows the linear regression of V_F* vs $\bar{\phi}$ for steady-state waves fronts (from Figure 1C).

To quantify correlation between V_F* and $\bar{\phi}$ in this case, we calculated values of both parameters for each point of the epicardial surface. Figure 3B and 3C show respective spatial maps of the localized values of $\bar{\phi}$ and V_F*. Note the narrow, nearly vertical band of large positive $\bar{\phi}$ (red) surrounded by saddle-shaped blue region of negative net angles. This specific spatial pattern represents a signature of subsurface wavefront orientations during epicardial point stimulation. Although the V_F* map (Figure 3C) uses a different color scheme, it bears a striking similarity with $\bar{\phi}$ map shown in Figure 3B.

Figure 3D shows a correlation plot derived from the 2 maps in Figure 3B and 3C. Although the propagation in this case is nonstationary, the correlation is very similar to that observed for the case of steady-state plane waves (dashed line). This indicates that OAP upstroke morphology is a reliable predictor of wavefront orientation not only during steady-state propagation but also during continuous wavefront transformation.

OAP Upstroke Dependence on Subsurface Wavefront Orientation: Experimental Studies

To test the predictions of the model experimentally, we conducted optical mapping experiments in isolated swine right ventricle preparations. In these experiments, we examined OAP upstroke morphologies for wavefronts produced by both line stimulation (parallel and perpendicular to epicardial fibers) and point stimulation (epicardial and endocardial).

Line Stimulation

To initiate quasi-plane waves with a positive $\bar{\phi}$ (see Figure 1A), we used a line electrode sutured to the epicardium, oriented perpendicular to the apparent epicardial longitudinal fiber direction. Figure 4A shows a V_F* map and corresponding isochrone map obtained from a swine right ventricular preparation in one such experiment. As can be seen from the spacing of the isochrones, after 20 ms the wavefront became linear and acquired stationary speed. The V_F* map (Figure 4A) showed random short-scale variations with the average of 0.385 (V_F*=0.385±0.088, n=1856 pixels). The fact that the average was <0.5 is consistent with the with model predictions of a positive $\bar{\phi}$. Figure 4B shows corresponding V_F* and isochrone maps obtained in the computer simulation for this particular case. The simulated value (V_F*=0.370) is close to the experimentally observed value. Equivalent results were obtained in 2 other experiments where the line electrode was oriented perpendicular to the surface fibers.

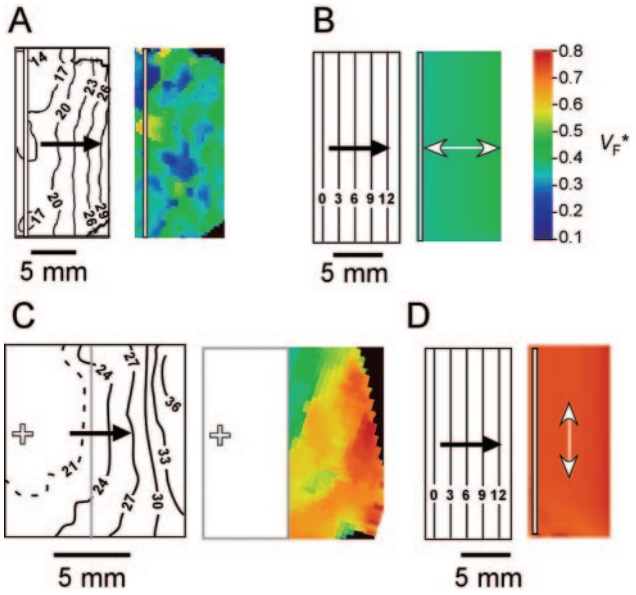

Figure 4. V_F* maps during steady-state lateral plane wavefront propagation in the longitudinal and transverse surface fiber directions. White arrows represent the fiber direction on the surface. Black arrows indicate the direction of lateral wavefront propagation. A, Experimental V_F* and surface isochrone maps for a plane wave propagating in the longitudinal surface fiber direction. Vertical white bar indicates the line stimulation site. B, Corresponding computer simulation. C, Experimental surface isochrone and V_F* maps for a wavefront propagating in transverse surface fiber direction. (The wavefront was induced by point stimulation that, at a distance of ≈5 mm from the recording site, indicated by a white cross.) D, Corresponding surface isochrone and V_F* maps for computer simulation.

To estimate V_F* values with negative $\bar{\phi}$, we used the experimental and computational fact that during epicardial point stimulation, a wavefront propagating across fibers (ie, in the transverse fiber direction) rapidly becomes a steady-state lateral plane wave. The isochronal map in Figure 4C shows a stationary propagating plane wave formed at a distance ≈5 mm from the point stimulation site. In this region, V_F* is significantly greater than 0.5 (V_F*=0.65±0.10; n=658 pixels), which is characteristic for negative $\bar{\phi}$. This result is in relatively good agreement with computer simulations (V_F*=0.78; see Figure 4D as well as Figure 1B).

Epicardial Point Stimulation

Figure 5A, 5B, and 5C depict an isochronal map, OAP upstrokes, and V_F* map obtained in a representative swine RV preparation after epicardial point stimulation. The experimental data are in excellent agreement with theory (compare Figure 5 with Figure 3). As in computer simulations, at site a, near the point stimulation, the experimentally recorded upstroke has relatively low value of V_F* (compare Figure 5B with 3A). At site b, as measured along the apparent transverse surface fiber direction, V_F* increased and the upstroke morphology assumed a more symmetric sigmoidal shape, which indicated a wavefront oriented perpendicular to the surface. At site c, further away from the stimulation site V_F* increased even more, giving rise to an upstroke with unusually long foot, which suggested a wavefront oriented toward the epicardium.

The experimental V_F* map for this experiment is shown in Figure 5C. This map is in excellent agreement with the theoretically predicted V_F* map in Figure 3B. Similar to the theoretically derived map, it has a relatively narrow band extending from the stimulation site in the approximate direction of surface fibers, with lower V_F* values, indicating a wavefront oriented away from the surface (blue/green regions in panel C). In the transverse surface fiber direction, we observe V_F*>0.5, indicating a wavefront oriented toward the surface (yellow/orange/red regions in C), as predicted by the model.

Similar V_F* patterns were observed in all experiments (n=8). Figure 6A shows optical mapping results for 4 additional swine right ventricular preparations in which the epicardium was subjected to point stimulation. Although there is considerable heterogeneity in these V_F* maps, likely attributable to inherent differences in the experimental preparations themselves, all V_F* maps show small values (indicated in blue and green) for V_F* along the approximate surface fiber direction, with significantly larger values (indicated in yellow, orange, and red) for V_F* in the transverse fiber direction. Figure 6B shows 4 V_F* maps from the same preparation. This experiment indicates that as the point stimulation site is moved on the epicardium, the V_F* pattern moves with stimulation site, as predicted by theory.

The Table summarizes a linear regression analysis for the increase in V_F* with distance from the stimulation site in the transverse surface fiber direction for both the computer simulation in Figure 3C and epicardial point stimulation experiments (n=8). The Table shows a high correlation (R^2>0.8) for both simulations and all but 1 of the 8 experiments in the swine right ventricle.

Endocardial Point Stimulation

During endocardial point stimulation (n=3), epicardial recordings reproducibly showed optical upstrokes with a long foot (V_F*≈0.8), fully consistent with theoretical predictions (see online Figure VII). A similar upstroke morphology was

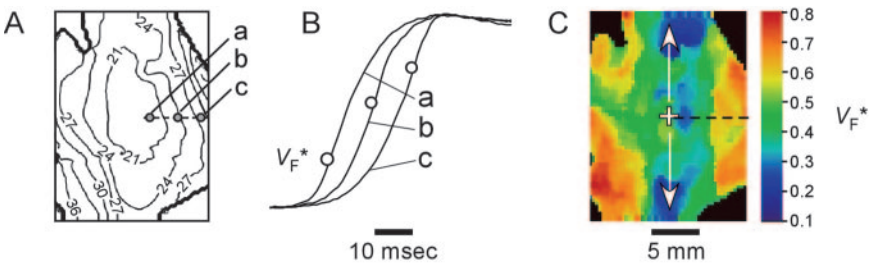

Figure 5. OAP upstroke morphology and V_F* map after epicardial point stimulation in experiment. A and B, Isochrone map and OAP upstroke morphology at sites a, b, and c. C, V_F* map for the same experiment. White cross denotes the point stimulation site. White arrows indicate the longitudinal fiber direction on the surface.

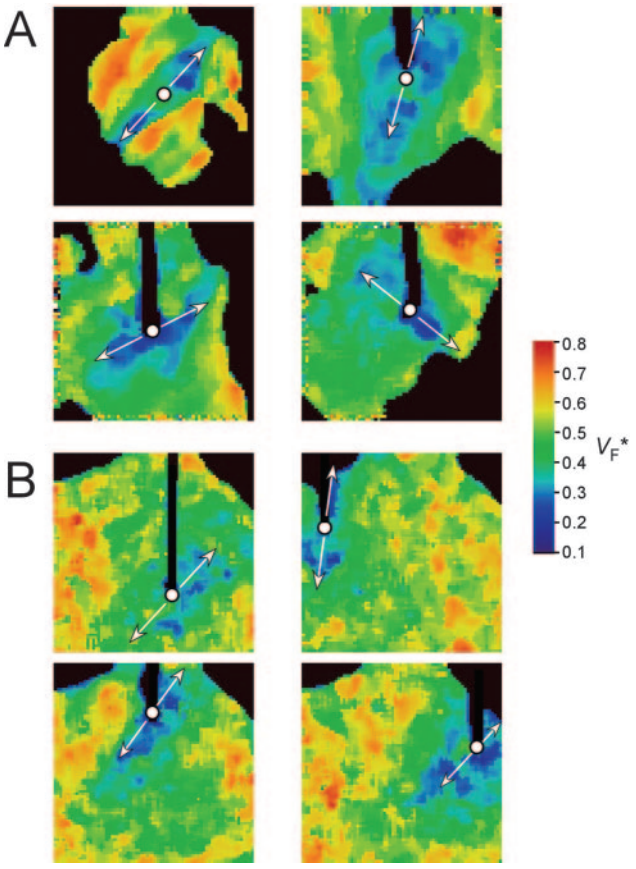

Figure 6. Epicardial stimulation and resulting V_F* maps. A, V_F* maps for 4 different preparations in which point stimulation was applied to the epicardium. In 3 of the maps, the stem of the stimulation electrode is visible. B, V_F* maps obtained from an additional preparation where the stimulation site was moved to 4 different locations on the epicardium. White circles mark stimulation sites. White arrows denote the apparent local epicardial fiber direction as determined from the initial expanding elliptical wavefront.

apparent in an earlier study.[12] Its origin, however, was not understood at the time.

Discussion

In this study, we used a combination of computer modeling and optical mapping experiments to establish the quantitative relationship between OAP upstroke morphology and subsurface wavefront orientation. We developed a procedure that could be applied both in computer simulations and animal experiments for producing excitation fronts with various orientations with respect to the surface. Using this procedure, we demonstrated that the level at which the rate of rise of the OAP reaches a maximum, V_F*, is linearly related to the optically weighted mean angle of the excitation wavefront with respect to the heart surface, $\bar{\phi}$. This finding suggests that optical upstroke morphology can be an accurate predictor of subsurface wavefront orientation.

Linear Regression Analysis for the Increase in V_F*

Experiment No.	Slope (V_F*/mm)	Intercept (V_F*)	R^2
Computer Simulation	0.0246	0.457	0.818
1	0.0541	0.269	0.874
2	0.0354	0.249	0.962
3	0.0319	0.238	0.942
4	0.0329	0.302	0.825
5	0.0198	0.444	0.215
6	0.0437	0.407	0.801
7	0.0428	0.245	0.861
8	0.0465	0.216	0.954
Mean	0.0384	0.2963	0.7934

To verify theoretical predictions, we conducted optical mapping experiments in isolated swine right ventricle preparations. We discovered that plane waves propagating along myocardial fibers produced upstrokes such that V_F*<0.5, which is consistent with the theoretical prediction for negative subsurface angles. Similarly good agreement with the theory (ie, V_F*>0.5) was obtained for plane waves propagating in perpendicular direction with positive subsurface angles. Finally, during epicardial point stimulation, we discovered characteristic saddle-shaped V_F* maps that were in excellent agreement with theoretically predicted changes in the subsurface wavefront angle during its expansion. These data provide strong evidence that the shape of optical upstroke contain useful information about 3D organization of excitation front and can become a novel useful tool for the interpretation of optical mapping data.

Electrical Versus Optical Upstroke

It has been demonstrated in several studies that fluorescent signal generated by fast voltage-sensitive dyes such as di-4-ANEPPS is proportional to changes in the transmembrane potential. Windisch et al have shown that optical upstrokes measured from single isolated cells can be as fast as, or even faster than, electrical upstrokes recorded using transmembrane microelectrodes.[13] Similarly, when comparing electrical and optical recordings in cardiac myocyte monolayers, identical upstroke durations have been obtained.[14] In 3D tissue preparations, however, optical upstrokes can be almost an order of magnitude longer than electrical upstrokes recorded from the same location using microelectrodes.[7,15,16]

There are several factors responsible for this discrepancy between electrical and optical upstroke duration.[17] Some of them are determined exclusively by the optical sensor (eg, pixel size, acquisition speed, and depth of field) and can potentially be corrected with improved technology (eg, reduced pixel size, higher acquisition speeds, and smaller depth of field). Theoretical analysis shows, however, that there is also a significant intrinsic factor, namely the scattering of light by myocardial tissue, that cannot be readily eliminated.[7,18] In thick tissues, because of light scattering, the optical upstroke will remain significantly prolonged even if imaging is performed on an infinitesimally small region on the heart surface. Our study shows, however, that this intrinsic prolongation is not always a problem that needs to be eliminated. In many cases, it can be used for extracting important 3D information about subsurface wavefront orientation.

The optical upstroke in 3D preparations is not only significantly longer but also has a significantly different shape than electrical upstroke. It is well established that the

foot of the electrical upstroke is determined by the passive cable properties of myocardial fibers, whereas the fast inward current often determines the maximal rate of change of the electrical upstroke ($\dot{V}_{max}$). Electrical upstrokes do manifest anisotropic differences in observed morphology (eg, the longitudinal and transverse dependence of τ-foot and $\dot{V}_{max}$ because of directional differences in the effective membrane capacitance caused by the asymmetric arrangement of gap junctions[11,19]). These anisotropic differences in electrical upstroke morphology do not, in general, have a counterpart in optical upstroke morphology. Our study shows that the shape of optical upstroke is determined primarily by the wavefront orientation with respect to the surface and has little or no correlation with the electrical upstroke (see Hyatt et al[7] and online Figures V and VI).

OAP Upstroke Morphology and Surface Conduction Velocity Measurements in Myocardium

Experimental measurements of conduction velocity in 3D myocardium are commonly performed using data from electrode array or optical mapping of electrical activity on the heart surface.[20–24] It is clear, however, that surface activation maps will not, in many cases, reflect the actual conduction velocity of the 3D electrical wavefront. For example, if a plane wavefront has a velocity vector of magnitude υ and angle $\bar{\phi}$ with respect to the surface, one will measure an apparent propagation velocity equal to $\upsilon/\cos(\bar{\phi})$ on the surface. As $\bar{\phi}$ approaches $+90°$ or $-90°$ (ie, a "breakthrough" on the surface), the calculated conduction velocity on the surface will approach infinity. Therefore, locations where the subsurface wavefront is at an angle other than $\approx 0°$ with respect to the surface cannot be used reliably for measurements of conduction velocity.

Improved measurements of conduction velocity on the surface of 3D myocardium can be achieved by identifying areas where the excitation front propagates parallel to the surface ($\bar{\phi}=0°$). Our findings provide a novel tool for identifying such areas. We discovered that wavefronts propagating parallel to the surface produce OAP upstrokes with $V_F^* \approx 0.5$. Thus, measuring conduction velocity exclusively in such regions should significantly improve the accuracy of such measurements in 3D ventricular myocardium.

Study Limitations

In our computer simulations, we used a monodomain model of electrical propagation with Neumann boundary conditions. Thus, our model does not account for the tissue–bath interface present in our experiments. Bidomain models reported in the literature suggest that boundary conditions at the tissue–bath interface may affect wavefront orientation near the epicardium[6] and may have an impact on the dynamics of scroll-wave reentry.[25] Nonetheless, good agreement between our experiments and model predictions suggests that errors attributable to neglecting tissue–bath interface effects were small.

In the tissue region immediately surrounding the epicardial stimulation site, however, we did detect minor discrepancies between theory and experiment. In many experiments, V_F^* was somewhat larger near the stimulation site than at distal sites along the longitudinal surface fiber direction (see Figure 5C). In contrast, in computer simulations, V_F^* was always smallest in the stimulation site region. This discrepancy may be attributable to virtual electrode effects[26–29] not reproduced by our monodomain model. A bidomain model may, therefore, provide better predictions near the stimulation site. In regions distal to the stimulation site, however, both models should provide nearly equivalent results.

Our computer simulations also did not take into account tissue heterogeneities (eg, fatty and connective tissue, electrical heterogeneities), tissue variations in voltage-sensitive dye staining, and dye photobleaching. It is important to note, however, that our experiments were performed in heart tissue possessing such heterogeneities, and yet these experiments were still in good agreement with computer simulations. Consequently, although our computer simulations represent a degree of simplification, these simulations provide indirect but convincing verification of our experimental work. We also note that our model cannot make accurate predictions of subsurface wavefront orientation at wavefront collision sites. At such sites, the colliding waves will result in a single, cusp-shaped wavefront with ill-defined orientation with respect to the heart surface.

Finally, for verification of our findings it would clearly be advantageous if the angle $\bar{\phi}$ could be directly measured not only in computer models but in tissue experiments as well. Such measurements, however, would require obtaining transmural isochrones at submillimeter resolution. To our knowledge, this currently exceeds the capabilities of conventional intramural mapping based on plunge electrodes, where the distance between recording sites is often >0.5 mm.[30–32] Such measurements should become a subject of future studies when adequate techniques become available.

Acknowledgments

This work was supported, in part, by National Heart, Lung, and Blood Institute grants 1RO1-HL071635-01, 2POI-HL39707 (to A.M.P. and S.F.M.), RO1-HL60843 (to C.J.H., F.J.V., and C.W.Z.), and grant P20-RR016457 (to F.J.V.) from the Biomedical Research Infrastructure Networks program of the National Center for Research Resources, National Institutes of Health.

References

1. Streeter, DD Jr, Spotnitz HM, Patel DP, Ross, J Jr, Sonnenblick EH. Fiber orientation in the canine left ventricle during diastole and systole. *Circ Res.* 1969;24:339–347.
2. Armour JA, Randall WC. Structural basis for cardiac function. *Am J Physiol.* 1970;218:1517–1523.
3. Pollard AE, Burgess MJ, Spitzer KW. Computer simulations of 3D propagation in ventricular myocardium. Effects of intramural fiber rotation and inhomogeneous conductivity on epicardial activation. *Circ Res.* 1993;72:744–756.
4. Keener JP, Panfilov AV. Three-dimensional propagation in the heart: the effects of geometry and fiber orientation on propagation in myocardium. In: Zipes DP, Jalife J, eds. *Cardiac Physiology: From Cell to Bedside*. Philadelphia, Pa: WB Saunders; 1995:335–347.
5. Colli Franzone P, Guerri L, Taccardi B. Potential distributions generated by point stimulation in a myocardial volume: simulation studies in a model of anisotropic ventricular muscle. *J Cardiovasc Electrophysiol.* 1993;4:438–458.
6. Henriquez CS, Muzikant AL, Smoak CK. Anisotropy, fiber curvature, and bath loading effects on activation in thin and thick cardiac tissue

preparations: simulations in a three-dimensional bidomain model. *J Cardiovasc Electrophysiol.* 1996;7:424–444.
7. Hyatt CJ, Mironov SF, Wellner M, Berenfeld O, Popp AK, Weitz DA, Jalife J, Pertsov AM. Synthesis of voltage-sensitive fluorescence signals from three-dimensional myocardial activation patterns. *Biophys J.* 2003; 85:2673–2683.
8. Fenton F, Karma A. Vortex dynamics in three-dimensional continuous myocardium with fiber rotation: filament instability and fibrillation. *Chaos.* 1998;8:20–47.
9. Berenfeld O, Pertsov AM. Dynamics of intramural scroll waves in three-dimensional continuous myocardium with rotational anisotropy. *J Theor Biol.* 1999;199:383–394.
10. Muzikant AL, Henriquez CS. Paced activation mapping reveals organization of myocardial fibers: a simulation study. *J Cardiovasc Electrophysiol.* 1997;8:281–294.
11. Spach MS, Heidlage JF, Darken ER, Hofer E, Raines KH, Starmer CF. Cellular Vmax reflects both membrane properties and the load presented by adjoining cells. *Am J Physiol.* 1992;263:H1855–H1863.
12. Efimov IR, Cheng Y. Optical mapping of cardiac stimulation: fluorescent imaging with a photodiode array. In: Candido, C, Rosenbaum, DS, eds. *Quantitative Cardiac Electrophysiology*. New York: Marcel Dekker Inc; 2002:583–622.
13. Windisch H, Ahammer H, Schaffer P, Muller W, Platzer D. Optical multisite monitoring of cell excitation phenomena in isolated cardiomyocytes. *Pflugers Arch.* 1995;430:508–518.
14. Fast VG, Kleber AG. Microscopic conduction in cultured strands of neonatal rat heart cells measured with voltage-sensitive dyes. *Circ Res.* 1993;73:914–925.
15. Gray RA. What exactly are optically recorded "action potentials"? *J Cardiovasc Electrophysiol.* 1999;10:1463–1466.
16. Bray MA, Wikswo JP. Examination of optical depth effects on fluorescence imaging of cardiac propagation. *Biophys J.* 2003;85:4134–4145.
17. Girouard SD, Laurita KR, Rosenbaum DS. Unique properties of cardiac action potentials recorded with voltage- sensitive dyes. *J Cardiovasc Electrophysiol.* 1996;7:1024–1038.
18. Ding L, Splinter R, Knisley SB. Quantifying spatial localization of optical mapping using Monte Carlo simulations. *IEEE Trans Biomed Eng.* 2001; 48:1098–1107.
19. Spach MS, Dolber PC, Heidlage JF, Kootsey JM, Johnson EA. Propagating depolarization in anisotropic human and canine cardiac muscle: apparent directional differences in membrane capacitance. A simplified model for selective directional effects of modifying the sodium conductance on Vmax, tau foot, and the propagation safety factor. *Circ Res.* 1987;60:206–219.
20. Morley GE, Vaidya D, Samie FH, Lo C, Delmar M, Jalife J. Characterization of conduction in the ventricles of normal and heterozygous Cx43 knockout mice using optical mapping. *J Cardiovasc Electrophysiol.* 1999;10:1361–1375.
21. Choi BR, Liu T, Salama G. The distribution of refractory periods influences the dynamics of ventricular fibrillation. *Circ Res.* 2001;88: e49–e58.
22. Eloff BC, Lerner DL, Yamada KA, Schuessler RB, Saffitz JE, Rosenbaum DS. High resolution optical mapping reveals conduction slowing in connexin43 deficient mice. *Cardiovasc Res.* 2001;51: 681–690.
23. Bayly PV, KenKnight BH, Rogers JM, Hillsley RE, Ideker RE, Smith WM. Estimation of conduction velocity vector fields from epicardial mapping data. *IEEE Trans Biomed Eng.* 1998;45:563–571.
24. Ni Q, MacLeod RS, Lux RL, Taccardi B. A novel interpolation method for electric potential fields in the heart during excitation. *Ann Biomed Eng.* 1998;26:597–607.
25. Sambelashvili A, Efimov IR. Dynamics of virtual electrode-induced scroll-wave reentry in a 3D bidomain model. *Am J Physiol.* 2004;287: H1570–H1581.
26. Roth BJ, Wikswo, JP Jr. Electrical stimulation of cardiac tissue: a bidomain model with active membrane properties. *IEEE Trans Biomed Eng.* 1994;41:232–240.
27. Knisley SB, Hill BC, Ideker RE. Virtual electrode effects in myocardial fibers. *Biophys J.* 1994;66:719–728.
28. Efimov IR, Cheng Y, Yamanouchi Y, Tchou PJ. Direct evidence of the role of virtual electrode-induced phase singularity in success and failure of defibrillation. *J Cardiovasc Electrophysiol.* 2000;11:861–868.
29. Muzikant AL, Henriquez CS. Bipolar stimulation of a three-dimensional bidomain incorporating rotational anisotropy. *IEEE Trans Biomed Eng.* 1998;45:449–462.
30. Deale OC, Ng KT, Kim-Van Housen EJ, Lerman BB. Calibrated single-plunge bipolar electrode array for mapping myocardial vector fields in three dimensions during high-voltage transthoracic defibrillation. *IEEE Trans Biomed Eng.* 2001;48:898–910.
31. Arnar DO, Bullinga JR, Martins JB. Role of the Purkinje system in spontaneous ventricular tachycardia during acute ischemia in a canine model. *Circulation.* 1997;96:2421–2429.
32. Pogwizd SM, Corr PB. Mechanisms underlying the development of ventricular fibrillation during early myocardial ischemia. *Circ Res.* 1990; 66:672–695.